DOI: 10.32615/ps.2020.016 PHOTOSYNTHETICA 58 (SI): 622-637, 2020

Special issue in honour of Prof. Reto J. Strasser

Phenotyping with fast fluorescence sensors approximates yield component measurements in pepper (*Capsicum annuum* L.)

S. LENK[*,+], J.A. DIELEMAN[**], V. LEFEBVRE[***], E. HEUVELINK[#], J.J. MAGÁN[##], A. PALLOIX[***,†], F.A. VAN EEUWIJK[###], and A. BARÓCSI[*]

Department of Atomic Physics, Budapest University of Technology and Economics, Budafoki út 8, H-1111 Budapest, Hungary[*]
Wageningen University & Research, Business Unit Greenhouse Horticulture, PO Box 644, 6700 AP Wageningen, The Netherlands[**]
INRAE, UR 1052 GAFL Genetics and Breeding of Fruit and Vegetables, F-84143 Montfavet Cedex, France[***]
Wageningen University & Research, Horticulture and Product Physiology Group, Wageningen, The Netherlands[#]
Experimental Station of Cajamar Foundation, Paraje Las Palmerillas – El Ejido, Almería, Spain[##]
Wageningen University and Research, Biometris Applied Statistics, P.O. Box 100, 6700 AA Wageningen, The Netherlands[###]

Abstract

Molecular breeding, a powerful technique to increase crop yield, tries to predict yield by crop growth models with genotype specific, environment-independent yield components and environmental indices as inputs. A fluorescence-trait-based approach is presented to approximate some costly and time-consuming measurements of yield components. Temporal monitoring of chlorophyll *a* fluorescence resulted in fluorescence traits with high heritability (0.60–0.82) that could act as proxies for model inputs. Medium-sized *Pearson*'s correlations were calculated between fluorescence traits, light-use efficiency (LUE), and fruit related parameters up to 0.53. Multi-trait quantitative trait locus (QTL) analyses identified genomic regions of pepper (*Capsicum annuum* L.) involved in the phenotypic variation of the fluorescence traits. Fluorescence QTLs found on linkage groups P6, P7, and P11 corresponded to QTLs for number of fruits, partitioning into fruits, and LUE. Fluorescence parameters within 1 min of the fluorescence response curve can thus be useful to approximate yield component traits.

Additional key words: complex trait; genotypic heritability; intelligent fluorosensor; plant phenotyping.

Introduction

Molecular breeding has become a powerful technique in present-day agriculture to increase yield of crop plants (Richards *et al.* 2002). To sustain and accelerate increase in crop yield, breeding companies need to improve their understanding of the relationship between genotype and phenotype. With the development of extremely fast

Received 30 August 2019, *accepted* 13 February 2020.
[+]Corresponding author; e-mail: barocsi@eik.bme.hu
Abbreviations: CM334 – 'Criollo de Morelos 334' pepper cultivar; DC – direct (unmodulated, or continuous) induction; DM_{fruit}, DM_{leaf}, DM_{stem}, DM_{tot} – dry mass of fruit, leaf, stem, and total plant (without root), respectively; DS – device server; E – environmental condition; F' – fluorescence from actinic-light-acclimated leaf; F_0, F_0' – minimal level of fluorescence from dark- and light-acclimated leaf, respectively; F_0'1, F_0'2 – the F_0' during far-red pulses; $F_0{}'^{calc}1$, $F_0{}'^{calc}2$, $F_0{}'^{calc}3$ – calculated F_0' at 60, 117, and 177 s, respectively; F_{690}, F_{735} – total fluorescence measured at 690 and 735 nm, respectively; F_m, F_m'' – maximal fluorescence in dark-acclimated state at 30 and 240 s, respectively; F_m'1, F_m'2, F_m'3 – maximal fluorescence in light-acclimated state at 60, 117, and 177 s, respectively; F_{PAM} – modulated fluorescence measured broadband; F_q'1, F_q'2, F_q'3 – difference of F_m' and actinic fluorescence from light-acclimated leaf at 60, 117, and 177 s, respectively; FR – far-red; F_v – variable fluorescence from dark-acclimated leaf; F_v'1, F_v'2, F_v'3 – variable fluorescence from light-acclimated leaf at 60, 117, and 177 s, respectively; g – genotype index; G – genotypic composition; H^2 – heritability; IFS – intelligent fluorosensor; LAI – leaf area index; LUE – light-use efficiency; N_{fruit} – number of fruits; OJIP – transient steps during the fast fluorescence rise; P1 to P12 – pepper linkage groups 1 to 12; PAM – pulse amplitude modulation; PAR_{int} – intercepted photosynthetically active radiation; QTL, QTLs – quantitative trait locus, or loci; RCB – randomized complete blocks; RIL – recombinant inbred line; RM – radio module; SP2, SP3 – locations of phenotyping experiments; SNP – single nucleotide polymorphism; YW – 'Yolo Wonder' pepper cultivar; η_{fruit} – partitioning into fruits.
Acknowledgements: The research leading to these results has received funding from the European Community's Seventh Framework Programme (FP7/2007-2013) under grant agreement no. KBBE-2008-211347 (SPICY). S. Lenk and A. Barócsi were also supported by the National Research, Development and Innovation Fund of Hungary within the Quantum Technology National Excellence Program no. 2017-1.2.1-NKP-2017-00001 (HunQuTech).
[†]A. Palloix passed away on 8 March 2016.

high-throughput genotyping equipment, high-throughput physiology and phenotyping is now often regarded as a major bottleneck in the breeding of new varieties (Furbank 2009). Thus, plant phenotyping has received considerable attention (Kolukisaoglu and Thurow 2010). Phenotyping can be aimed at the external appearance of the above-ground plant parts (van der Heijden *et al.* 2012, Song *et al.* 2014), at the root system (Ruts *et al.* 2013, Kuijken 2015) as well as at internal structures and processes (Bürling *et al.* 2013). The process of photosynthesis forms the basis for plant growth and yield (Barbagallo *et al.* 2003). Fluorescence type measurements give a deeper insight of plant physiology related to photosynthetic activity, efficiency and apparatus (Maxwell and Johnson 2000) and find an increasing number of applications (Bąba *et al.* 2019). Analysis of chlorophyll *a* (Chl) fluorescence transients has successfully been applied in distinguishing plant species (Mishra *et al.* 2009, Tyystjärvi *et al.* 2011). Correlations between fluorescence parameters and yield components have been found in case of barley with the highest values between plant mass and photochemical quenching (Marcial and Sarrafi 1996). Quantitative trait loci (QTLs), regions with DNA variation that is associated with phenotypic trait variation, for fluorescence related traits have also been identified in *Arabidopsis* (Flood *et al.* 2016, van Rooijen *et al.* 2017).

Crop growth models have proven to be excellent tools to predict crop yield from crop physiological knowledge under different management environmental conditions (Boote *et al.* 2001, Marcelis *et al.* 2006). The earlier implementations of crop growth models did not take into account genetic differences. Genotype specific predictions of yield by crop growth models are problematic because of the fact that genotypic differences in yield are environment dependent. This phenomenon of yield differences between genotypes being a function of the environmental conditions is called genotype by environment interaction (G × E; van Eeuwijk *et al.* 2016). For the prediction of G × E in yield by ecophysiological process-based crop simulation models, these models need to be fed with genotype specific physiological input traits that themselves are not sensitive to G × E. The crop growth model transforms the physiological inputs together with environmental inputs into yield with G × E. A further level of complexity can be added by making the physiological inputs functions of underlying genes or QTLs. For examples of this type of models, *see* Bertin *et al.* (2010), Yin *et al.* (2004, 2005), van Eeuwijk *et al.* (2016), and Bustos-Korts *et al.* (2016).

A crop growth model is defined by its inputs and outputs and a set of functions that transform the inputs into outputs. The inputs are physiological traits and environmental indices describing the growing conditions. The physiological inputs often require costly and time-consuming phenotyping, *i.e.*, measurements, especially so when the aim of the phenotyping is to characterize a population or panel of genotypes. Crop growth models vary in complexity. Some very basic physiological inputs for most crop growth models are growth rate of leaf area index (LAI), light-use efficiency (LUE), and partitioning into fruits (η_{fruit}) that is the ratio of total fruit dry mass to total plant dry mass (van Ittersum *et al.* 2003). These yield components can be obtained by costly manual measurements. Alternatively, the component traits themselves or proxies to them could follow from nondestructive measurements of processes like photosynthesis or Chl fluorescence emission. Estimating component traits in such a way has advantages over destructive measurements. Less plants need to be grown as plants are kept intact and measurements can be repeated in time. New tools allowing large-scale automated phenotyping are necessary in the breeder's toolbox.

Optical techniques present new opportunities to develop novel phenotyping platforms that enable large-scale screenings of genotypes for several traits in multi-location field or greenhouse trials (Montes *et al.* 2007, Furbank and Tester 2011). There are several commercial instruments available in the market to determine Chl *a* fluorescence characteristics (examples are given in Barócsi *et al.* 2000, Strasser *et al.* 2000, Cerovic *et al.* 2012, and Schreiber *et al.* 2012). However, many available fluorescence screening techniques lack the capability of mass-measurement: either the applied method is slow thus the subsequent data evaluation is complicated and/or time consuming, or the recorded signal is only partial, or the apparatus is fixed and cannot be used on agronomic plants in growing conditions. A dedicated intelligent fluorosensor (IFS) instrumentation focuses on the potential for mass-measurements (*i.e.*, of many genotypes) allowing parallelization of several intelligent, autonomous fluorescence sensors with an appropriate time-reduced screening methodology and automated data preprocessing. This concept, illustrated in Fig. 1, the corresponding sensor system, and its reliability have been introduced by Barócsi (2013).

In this paper, the IFS system as a fast fluorescence tool was used to phenotype a pepper (*Capsicum annuum* L.) progeny with the aim to replace the costly and time-consuming measurements on yield components. The research formed part of the EU FP7 program 'SPICY' focusing on the early prediction and improvement of crop yield by means of (*1*) a suite of smart tools for molecular breeding, and (*2*) an integrated approach of QTL and crop growth modelling to predict the phenotypic response with genotypic information encapsulated in the model parameters (van Eeuwijk *et al.* 2010, Voorrips *et al.* 2010). The potential of this genotype-to-phenotype modelling has been illustrated by Chenu *et al.* (2009). A full discussion of this methodology is offered by Bustos-Korts *et al.* (2016).

Fluorescence is induced when a sample is illuminated by a set of light sources with spectral radiation falling in the plant's absorption range. Different wavelengths excite the plant's photosystems with different efficiencies (Pedrós *et al.* 2010) and difference in light conditions determines the light-harvesting capability of the photosystems. Basically, in dark-acclimated state, the photosynthesis is reduced and upon illumination with a saturating pulse, the fluorescence emission is increased to a higher maximum. Contrarily, in light-acclimated state the maximal fluorescence emission is lower upon the same saturating pulse (Strasser *et al.*

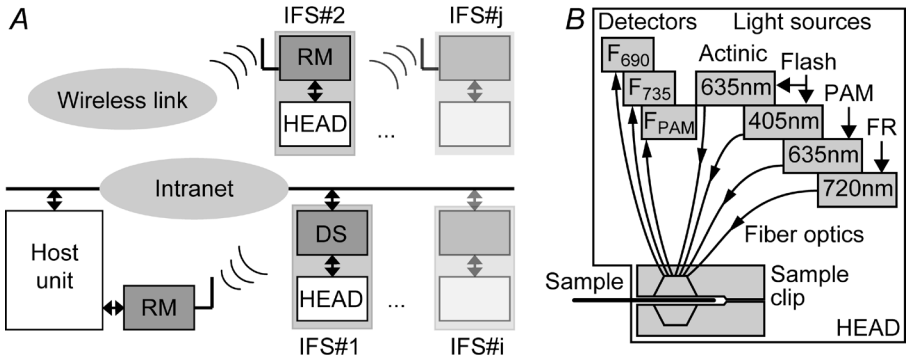

Fig. 1. (*A*) Block scheme of the IFS system. The data of the sensors are accumulated by the host unit. The measuring heads have either intranet (IFS#1) or wireless (IFS#2) connectivity to the host. HEAD – measuring head, DS – embedded device server, RM – 802.15.4 protocol based radio module. (*B*) Block scheme of the measuring head showing all different light sources and detection channels. Details are given in the text.

2000). The different acclimation states and the transitions between them are monitored by two different techniques using either direct (DC) induction of total fluorescence, or pulse amplitude modulated (PAM) induction of variable fluorescence. At the onset of the actinic light, a quasi-logarithmic sampling of the fast fluorescence rise following the dark-acclimated state allows capturing the transient responses related to the so called OJIP steps (Strasser *et al.* 1995, Barócsi 2013). The emitted total fluorescence is always proportional to the excitation intensity which changes by several orders of magnitude. To distinguish the variable component of fluorescence, the examinable light environment (determined by the actinic light driving the fluorescence kinetics and the saturating transient flashes) is separated from the modulated probing light so that only the portion of fluorescence excited by a low dose probing light (composed of short uniform pulses with low intensity) is measured by synchronous detection (Huot and Babin 2010).

Fluorescence of leaves originating from the fluorescing pigment Chl *a* consists of two bands with maxima in the red (near 685–690 nm, F_{690}), and far-red (near 730–740 nm, F_{735}) regions. Both fluorescence maxima are complex signatures influenced by many leaf and environment dependent factors (Buschmann 2007). Since the origins of F_{690} and F_{735} are different, additional information can be gained from the separate detection of the two maxima to improve the fluorescence-trait-based prediction. A major difference of the two bands is that the short wavelength fluorescence emission overlaps with the red absorption band of Chl *a* centered at 680 nm, hence, due to the resulting reabsorption, the F_{690}/F_{735} ratio of the two Chl *a* fluorescence maxima depends on the concentration of Chl *a* bound to one of the two photosystems in the leaf tissue (Buschmann 2007). At room temperature, Chl *a* fluorescence is emitted mainly from PSII but a small contribution is emitted from PSI as well in the spectral range above 700 nm depending on the stage of the light induced photosynthetic induction (Palombi *et al.* 2011). Thus, the short wavelength, red Chl *a* fluorescence band is not influenced significantly by PSI fluorescence which makes some contribution to the long-wavelength band reaching about 30–40% in the F_0 minimal fluorescence from dark-acclimated leaf in case of plants exhibiting C_3 photosynthetic pathways like pepper. For other fluorescence parameters, this contribution is significantly different, typically lower, *e.g.*, *ca*. 5–10% for F_m maximal fluorescence from dark-acclimated leaf (Pfündel 1998). Finally, far-red fluorescence is thought to have origin also from aggregate formation of light-harvesting complex of PSII (Miloslavina *et al.* 2008).

We investigated whether we can develop a fast protocol for measuring fluorescence traits, whether such fluorescence traits show consistent differences between genotypes, and whether these fluorescence traits can be related to yield and yield components by looking at *Pearson*'s correlations between genotypic means and collocation of QTLs. Our objective is firstly to assess whether our fluorescence measurements provide fast and cheap proxies to yield components and may replace costly yield components in crop growth models. Secondly, we aim at elucidating the genetic basis of yield variations by identifying QTLs for fluorescence that collocate with QTLs for yield and yield components.

Materials and methods

Plant material and experimental setup: The plant material used in the experiment consisted of a progeny of recombinant inbred lines (RIL) obtained from the cross between the sweet 'Yolo Wonder' (YW) and the pungent 'Criollo de Morelos 334' (CM334) pepper cultivars (Barchi *et al*. 2007, Bonnet *et al*. 2007) and was supplied by INRA (renamed INRAE in 2020), the French National Institute for Agricultural Research, Avignon. From the 297 genotypes (individual F5-lines) of the RIL progeny, 37 were selected for this experiment according to the data described in Barchi *et al*. (2007). The set of 37 lines showed a large variability of yield components with the same distribution shape than those of the whole 297 lines progeny. Together with the parents YW and CM334, and the first generation F1, the experiment consisted of 40 genotypes with 30 to 40 plants per genotype. The experiment, referred to as 'SP3', was located at EEFC, the Experimental Station of Cajamar Foundation, near El Ejido, Spain. Seeds were sown on 22 June 2010. Plantlets were planted on 28 July 2010. Plant density was approximately three plants per m^2. During cultivation, two stems per plant were kept. Side shoots were topped at the second internode, *i.e*., they had three leaves and three flowers (no flower was removed from the side shoots). At the start of the experiments, six plants per genotype were harvested destructively and the leaf area (of leaves with width > 2 cm) and dry mass of leaves and stem were recorded. During the experiment,

ripe fruits were harvested on six plants per genotype when they were at least 50% red and their number of fruits and fresh masses were recorded. Dry mass of some fruits was recorded to determine their dry matter content and used to estimate the dry mass of all harvested fruits. When a genotype reached the wire, six plants of that genotype were harvested destructively to measure leaf area, dry masses of stem, leaves, and fruit and the number of fruits. The experiment was ended on 14 December 2010, when the remaining genotypes were harvested.

The experiment was carried out in a plastic covered greenhouse with dimensions of 40-m column by 60-m row. The multi-span tunnel and rows were oriented east-west and north-south, respectively. There were 22 rows of 54 perlite bags with five plants per bag. The experiment was a randomized complete blocks (RCB) design consisting of two blocks, each containing all 40 genotypes. In each block, we set up one plot of 15 to 20 plants per genotype and the middle three plants of each plot were used as experimental plants. The rest served as guard plants on which no measurements were performed to avoid the border effect due to the neighbours.

Climate control inside the greenhouse was passive implying that there was no heating and CO_2 supply. Greenhouse air temperature, humidity, CO_2 concentration, outside temperature and inside radiation were recorded every 5 min. Average greenhouse air temperature throughout the experiment was 21.6°C, whereas the average radiation sum inside the greenhouse was 6.4 MJ m^{-2} d^{-1}.

QTL locations were compared to those found in an earlier large-scale phenotyping experiment at the same location and season, referred to as 'SP2' (Alimi *et al.* 2013a,b). Plant material for SP2 consisted of 149 genotypes of RIL progeny from YW × CM334, the parents YW and CM334 and F1. Of these, a set of 19 genotypes were present in both SP2 and SP3 experiments. Seeds were sown on 9 June 2009 and planted on 16 July 2009. The experiment ended on 14 December 2009. Climate control and data registration were identical to that in the later experiment with average greenhouse air temperature of 22.5°C and radiation sum of 6.2 MJ m^{-2} d^{-1}. Similarly, 22 rows of 54 perlite bags of five plants were placed and all 152 genotypes were placed in two blocks. In each block, one plot of 10 plants per genotype was placed, of which the middle three plants were used for measurements of plant development. The other seven plants were considered as guards on which no measurements were performed. Stems per plant, plant density, side shoot and fruit harvest conditions were identical to that in SP3.

Randomization schemes were made for both experiments following an RCB design. More details of the experimental designs at SP2 and SP3 can be found in Alimi *et al.* (2013a) and Barócsi (2013), respectively, but relevant differences are given in the Appendix. Genetic analysis of yield and physiological traits were performed in Alimi *et al*. (2013a).

Fluorescence measurements and sampling protocol: Measurements with the IFS instruments (Fig. 1; Barócsi 2013) were carried out between 5 and 24 October 2010. The 40 selected genotypes were measured according to a predefined sampling scheme which ensured that repeated measurements on the same genotype were made at different times of the day, at different plot locations and with different sensors to allow elimination of the resulting fixed effects in the following analysis. The first fully expanded leaf from top, being not shaded by other leaves, was selected for measurements. The fluorescence samplings were carried out by two IFS sensors having been preadjusted for optimal device parameters derived from previous experiments to allow uniform measurements (Barócsi 2013). The two sensors measured adjacent plots to minimize the effect of greenhouse location and allow faster sensor placement, and recorded 14 to 30 fluorescence data sets per genotype.

The fluorescence measurement protocol, described in detail by Barócsi (2013), is shown in Fig. 2 with the definition of the collected parameters. Herein, a relevant summary is given. A first dark acclimation shortened to 2 min was applied to the leaf sample to achieve a uniform initial condition for all samples. Within this period, the sample is illuminated by a far-red (FR) light pulse of 720 nm at irradiance of 4 W m^{-2} to get the minimum of original fluorescence, denoted as F_0'1 in this paper. This FR pulse was repeated at the end of actinic period to measure the minimum fluorescence of the light acclimated sample denoted as F_0'2 (identical to F_0' in the literature). Fluorescence response to the actinic light [excited by a laser diode of 635 nm with PPFD = 480 µmol m^{-2} s^{-1}] was recorded up to 3 min so that the true steady-state fluorescence was almost reached. At five time points, high intensity ('saturating') flashes were applied by combining the maximal available red laser power (*ca*. PPFD = 2,200 µmol m^{-2} s^{-1}) with that of a 405 nm LED source (providing *ca.* PPFD of 270 µmol m^{-2} s^{-1}). The given PPFD values were measured on a 4.5-mm diameter detector placed coaxially at the sample surface of the instrument.

Both IFS sensors are equipped with two DC detection channels measuring total temporal fluorescence signals F_{690} and F_{735} recorded at the two spectral bands of 690 and 735 nm. In addition, one of the two sensors (IFS#1) is equipped with a pulsed LED source of 635 nm modulated at 25 kHz and the corresponding synchronous detection channel to record the PAM signal F_{PAM} broadband covering the entire Chl *a* fluorescence spectrum from 680 to 760 nm. The synchronous source provides sampling pulses with duration of 1 µs and PPFD = 7.7 µmol m^{-2} s^{-1}. To improve signal-to-noise ratio, this PPFD is set to a significantly higher value than that common in PAM practice, yet it serves physiologically relevant information (Solti *et al.* 2014). The significance of the PAM recording is the possibility of comparison to other commercial instruments, and the direct recording of the original fluorescence F_0 and its minimal level (F_0'1 and F_0'2). It should be noted, that F_0 is the response solely to the sampling pulse for the PAM channel, whereas it is taken as the first measured fluorescence value after the onset of the actinic light for any of the DC channels.

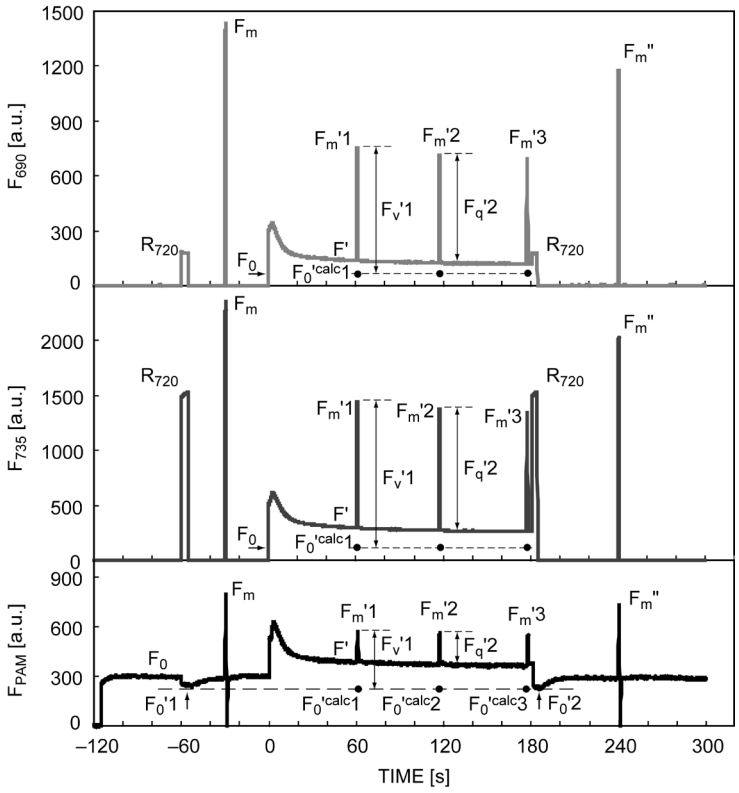

Fig. 2. Temporal scheme of the measuring protocol showing fluorescence response curves of a sample. F_{690} and F_{735} are the total fluorescence responses at 690 and 735 nm, respectively, and F_{PAM} is the modulated fluorescence response. Parameters F_0, $F_0'1$, $F_0'2$, F_m, F_m'' and F' as well as $F_m'i$, $F_v'i$, $F_q'i$ and $F_0^{'calc}i$ with $i \in \{1, 2, 3\}$ at time points $t_i \in \{60, 117, 177$ s$\}$ are discussed in the text. The 720-nm FR illumination results in a direct reflection R_{720} in both DC responses, and $F_0'1$ and $F_0'2$ in the PAM response.

Derivation of fluorescence parameters*:* Barócsi (2013) showed that the two instruments provide comparable results in case of the DC channels. Therefore, the combined dataset from IFS#1 and IFS#2 was used in the analysis yielding 913 independent DC measurements and the corresponding parameter sets. The following parameters were derived from the 690 and 735 nm DC fluorescence response curves according to Fig. 2: values measured at the light flashes given at – 30 s (F_m), 60 s ($F_m'1$), 117 s ($F_m'2$), 177 s ($F_m'3$), and 240 s (F_m''). Each flash contained several measurement points which were averaged. During the actinic light period (between 0 and 180 s), the response curve is smoothed with nonparametric smoothing. The fluorescence values before the flash light induced only by the actinic light (F' at 60, 117, and 177 s) were used to calculate $F_q'1$, $F_q'2$, and $F_q'3$, respectively, by taking the differences between the corresponding flash and F' values. $F_0^{'calc}1$, $F_0^{'calc}2$, and $F_0^{'calc}3$ were calculated using the formula from Baker and Rosenquist (2004), originally in Oxborough and Baker (1997):

$$F_0^{'calc}i = \frac{F_0}{\frac{F_m - F_0}{F_m} + \frac{F_0}{F_m'i}} \quad (1)$$

where index i can take values of $i \in \{1, 2, 3\}$ referring to the corresponding time points $t_i \in \{60, 117, 177$ s$\}$ of the fluorescence response.

As PAM detection was available only in sensor IFS#1 at the time of sampling, a single sensor dataset was used for evaluation with 448 independent PAM measurements and the corresponding parameter sets. In addition to the DC parameters listed above, the PAM signal gave the $F_0'1$ and $F_0'2$ data at times of the FR pulses before and after the actinic period, as well as the parameter F_0 obtained as the average of the dark response in the range of –100 to –60 s. The Appendix summarizes the calculated plant physiological parameters.

Derivation of crop model parameters: For yield prediction, a simple mechanistic crop model (rather than a regression model) with only a few genotype-specific parameters has been chosen that calculates biomass production based on daily light interception and utilization with an experimentally derived value for LUE (van Ittersum *et al.* 2003, Shibu *et al.* 2010). Yield was defined as the total fruit dry mass (DM_{fruit}), combining the harvested and unharvested fruits and expressed as dry mass per unit area [g m^{-2}]. Total plant dry mass (DM_{tot}) was calculated as the sum of dry masses of stem (DM_{stem}), leaves (DM_{leaf}), and fruits (both harvested and unharvested fruits). Fruit-related traits were the number of fruits produced (N_{fruit}, again both harvested and unharvested fruits) and η_{fruit}. For calculating $\eta_{fruit,g}$ for genotype g, the total fruit dry mass was divided by the total plant dry mass of genotype g, so that for yield:

$$DM_{fruit,g} = \eta_{fruit,g} \times DM_{tot,g} \quad (2)$$

This simple model requires three genotype-specific yield components, indexed for genotype g, which are leaf area index development rate $LAI_{rate,g}$, LUE_g, and $\eta_{fruit,g}$. All these components can be measured noting that the parameters themselves are still combined entities.

For example, LUE_g integrates underlying processes like leaf photosynthesis and respiration both having a large number of parameters which are not feasible to measure in large experiments. In this model, the total plant dry mass production for genotype *g* is given by the formula:

$$DM_{tot,g} = DM_{tot,g}(t_0) + \int_{t_0}^{t_1} LUE_g \times PAR_{int,g}(t)\, dt \quad (3)$$

defined at t_1 as the initial plant dry mass $DM_{tot,g}(t_0)$ plus the produced biomass between final and initial harvests at times t_1 and t_0, respectively. Here, LUE_g [g MJ^{-1}] is the biomass production per unit intercepted radiation, and $PAR_{int,g}(t)$ [MJ m^{-2} d^{-1}] is the daily intercepted radiation per unit area at time *t* for genotype g. LUE_g is assumed to be constant over time.

Ideally, radiation is expressed as photosynthetically active radiation (PAR). However, as global radiation was measured inside the greenhouse and the proportion of PAR in the global radiation varied due to cladding of the greenhouse, LUE_g was expressed per unit intercepted global radiation. To calculate $PAR_{int,g}(t)$, the daily values of leaf area index per unit soil area $LAI_g(t)$ [m^2 m^{-2}] at time *t* for genotype g were calculated as:

$$LAI_g(t) = LAI_g(t_0) + LAI_{rate,g} \times \int_{t_0}^{t} [T(\tau) - T_0]\, d\tau \quad (4)$$

starting at the initial value $LAI_g(t_0)$ and increasing linearly with slope $LAI_{rate,g}$ over thermal time. Thermal time is defined with the integral expression in Eq. 4. $LAI_g(t)$ depends on the average daily temperature $T(\tau)$ on day τ so that below a baseline temperature, set at T_0 = 10°C for all genotypes, the leaf area index does not expand (Marcelis *et al.* 2006). The daily intercepted radiation at time *t* for genotype g was then obtained as:

$$PAR_{int,g}(t) = [1 - e^{-\kappa\, LAI_g(t)}]\, PAR(t) \quad (5)$$

using Lambert-Beer's law with $LAI_g(t)$ and extinction coefficient of κ = 0.7 for all genotypes (Marcelis *et al.* 1998). Again, global radiation was substituted for PAR(*t*). Yield components for model inputs can be determined from experimental data for each genotype g. Dry mass of leaves, stems, and fruits were determined by drying plant organs for at least 48 h at 105°C in a ventilated oven. Leaf area was measured with a leaf area meter (*LI-3100C*, *LI-COR Inc*., Lincoln, NE, USA). Partitioning into fruits was calculated as the total fruit biomass divided by the total plant biomass at time t_1 of the final destructive harvest, according to Eq. 2: $\eta_{fruit,g} = DM_{fruit,g}/DM_{tot,g}$. The increase rate of leaf area index $LAI_{rate,g}$ was calculated as the ratio of the increase of leaf area index $LAI_g(t_1) - LAI_g(t_0)$ to the thermal time between the final and initial destructive harvests at times t_1 and t_0, respectively, according to Eq. 4.

Finally, the daily intercepted radiation was summed over the total growth period between $t_1 - t_0$ using Eq. 5, resulting in the total intercepted radiation per unit area. Then, LUE_g was estimated as the constant slope of total biomass production and total intercepted radiation at time t_1 of final harvest, according to Eq. 3:

$$LUE_g = \frac{DM_{tot,g} - DM_{tot,g}(t_0)}{\int_{t_0}^{t_1} PAR_{int,g}(t)\, dt} \quad (6)$$

Statistical analyses: Measurements of fluorescence parameters and crop parameters were all obtained at individual plant level, except for LUE which was calculated per plot. Following the experimental design of the SP3 experiment, genotypic means were predicted from the data per plant or plot using linear mixed models that corrected for position of the plant or plot in the greenhouse and, in case of fluorescent measurements, for the sensor, day and time of the day at which the measurements were taken. For further details, *see* Alimi *et al.* (2013a,b) on the phenotypic analyses, and Barócsi (2013) on genotypic means and statistical analyses of fluorescence parameters. For the set of 37 RIL genetic variances, plot error variances and broad sense heritabilities on a genotypic line mean basis were estimated. Heritability values range from zero if all of the observed differences between genotypes are environmental, to one meaning that all differences are genetic. Broad sense heritability is also interpreted as a measure of reproducibility of the differences between genotypes when the experiment would be repeated (Oakey *et al.* 2006).

Correlation analyses were also carried out (*1*) on fluorescence parameters to map the degree of their interdependencies, especially of similar parameters taken at various times in the measurement protocol, and (*2*) between fluorescence and crop growth parameters to identify possible relationships between fluorescence traits and yield components.

Finally, fluorescence parameters were subjected to QTL analysis to find out whether their QTLs would collocate with QTLs for yield and yield components. The genetic map of the progeny consisted of 455 markers, mainly SNPs (single nucleotide polymorphisms), distributed over 12 linkage groups called P1 to P12. For the fluorescence parameters, a multi-trait QTL analysis was performed following the methodology described by Boer *et al.* (2007). All analyses were carried out using *GenStat 16* (*VSN International*, Hemel Hempstead, UK). Similar parameters taken at various times in the measurement protocol were analysed together, *e.g.*, F_v'/F_m' at 60, 117, and 177 s. Rational parameters F_v'/F_m', F_q'/F_v', and F_q'/F_m' were also analysed together.

Results

The analyses focus on 37 genotypes of the RIL progeny, as they serve as an example of a breeding progeny in which selection for high yielding genotypes is done, based on fast nondestructive fluorescent measurements.

Correlations of raw data and predicted genotypic means tested on selected fluorescence parameters based on 448 independent PAM measurements are shown in Fig. 3.

Fig. 3*A*,*C* shows the correlation between parameters F_0'1 and F_0'2 for the measured raw and predicted mean values, respectively, yielding high squared correlation coefficients of $R^2 > 0.9$ in both data sets. Also, both the F_0'1 and F_0'2 values show strong correlation to the corresponding calculated F_0'^{calc}1 values for raw data (Fig. 3*B*) and predicted means (Fig. 3*D*) obtained using the formula of Eq. 1. As a consequence of the model-based prediction that improves variance structure, the correlation significantly increased for predicted genotypic means. Due to the measurement principle, F_0' cannot be derived directly from the DC measurements yielding the total fluorescence (instead, the direct reflection response R_{720} is recorded), but the calculated F_0'^{calc}i values can still be produced using the same formula (data not shown). For DC responses, F_0'^{calc}i is used to determine the variable fluorescence components F_v'*i*.

Fig. 4 presents the predicted value ranges and their distribution of the selected rational fluorescence parameters taken at different time points of the light-acclimated phase. In general, the genotypic mean values of F_v'/F_m', F_q'/F_v', and F_q'/F_m' were lower at 735 nm than that at 690 nm (Fig. 4*B–D*). The values of F_v/F_m and F_v'*i*/F_m'*i* at both 690 and 735 nm are measured to be higher than 0.83, the theoretical maximum (Baker 2008) due to the fact that the IFS measures total rather than variable fluorescence at its DC channels, which is changing with higher dynamics (Huot and Babin 2010). For both wavelengths, F_q'/F_v' and F_q'/F_m' increased over time. The genotypic means of the same fluorescence parameters measured with PAM technique were much lower than those measured at 690 and 735 nm (Fig. 4*A*). Again, parameters F_q'/F_v' and F_q'/F_m' increased over time, while there was a slight decrease in F_v'/F_m' over time.

Fig. 5*A*,*B* maps the pairwise correlations of genotypic mean values at different time points for rational parameters F_v'/F_m', F_q'/F_v', and F_q'/F_m' within response curves F_{735} and F_{PAM}. As seen, the values at different time points (60, 117, and 177 s) of any of the parameters of any responses tend to strongly correlate with an average *Pearson*'s correlation coefficient of $R = 0.95$ for each parameter group at a significance level of $p<0.001$ for all pairs. The correlation

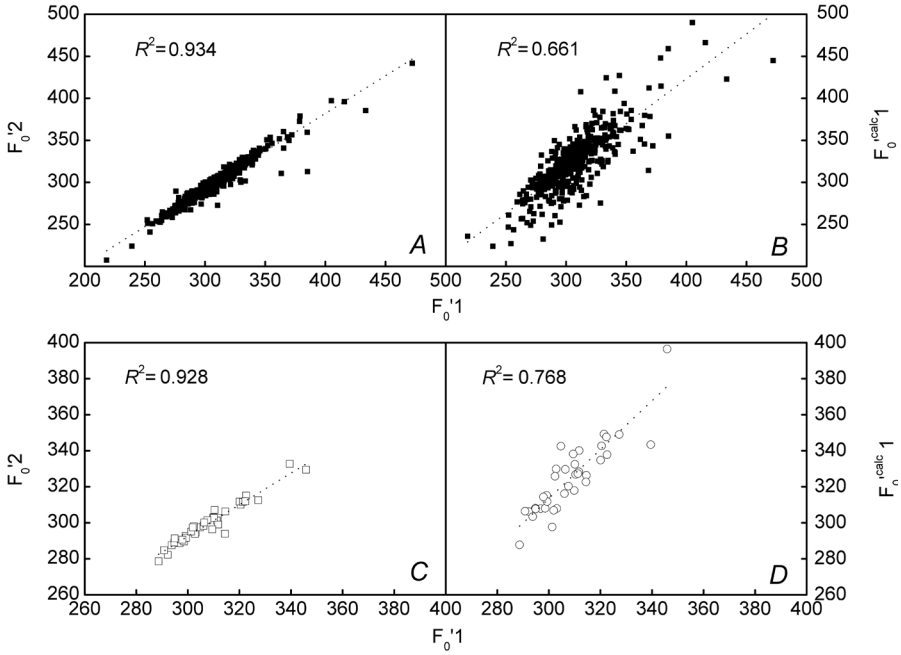

Fig. 3. Correlation of selected fluorescence parameters based on 448 independent PAM measurements taken by the IFS#1 device. F_0'1 and F_0'2 are the means of five or six measurement points, each. (*A*) Correlation between the measured F_0'1 and F_0'2 values. (*B*) Correlation of the F_0'1 measured values to the corresponding F_0'^{calc}1 values calculated using the formula of Eq. 1 according to Oxborough and Baker (1997). (*C*) Correlation of the predicted genotypic means of F_0'1 and F_0'2. (*D*) Correlation of the predicted genotypic means of F_0'1 and F_0'^{calc}1.

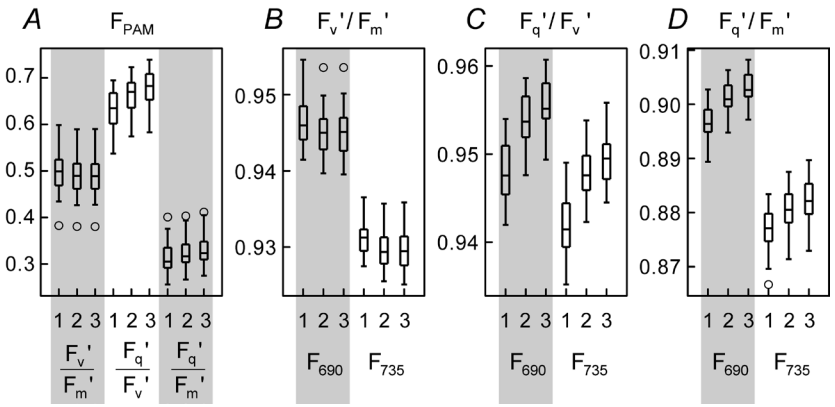

Fig. 4. Boxplots of genotypic means of PAM and DC fluorescence parameters predicted for 35 and 37 genotypes of a RIL progeny, respectively, obtained with the IFS instruments. (*A*) Parameters F_v'/F_m', F_q'/F_v' and F_q'/F_m' at 60 s (1), 117 s (2) and 177 s (3) of the PAM response. (*B–D*) Parameters F_v'/F_m', F_q'/F_v' and F_q'/F_m' at 60 s (1), 117 s (2) and 177 s (3) of F_{690} and F_{735} DC responses.

Parameter	F_v'/F_m'			F_q'/F_v'			F_q'/F_m'		
Time pair	1-2	1-3	2-3	1-2	1-3	2-3	1-2	1-3	2-3
A F_{735}	0.97	0.92	0.98	0.94	0.88	0.98	0.99	0.98	0.995
B F_{PAM}	0.998	0.995	0.999	0.96	0.93	0.98	0.97	0.95	0.990
Curve pair	690-735	690-PAM	735-PAM	690-735	690-PAM	735-PAM	690-735	690-PAM	735-PAM
C 1	0.81	0.34	0.41	0.77		0.48	0.85	0.43	0.52

Fig. 5. Pairwise correlation scatter plots of genotypic mean values for rational parameters F_v'/F_m', F_q'/F_v', and F_q'/F_m' with *Pearson*'s correlation coefficients *R* (significant at $p<0.001$) and correlation ellipses corresponding to confidence interval of 0.95. (*A*,*B*) Correlations at different time points within response curves F_{735} and F_{PAM} taken at 60 s (1), 117 s (2), and 177 s (3). F_{690} values are omitted as showing similar trends to those of F_{735}. (*C*) Correlations between similar fluorescence parameters obtained at identical time points at 60 s (1) with different measurement techniques. Time points 2 and 3 are omitted as showing similar trends to those at time point 1.

was the highest for the measurement pairs made at 117 and 177 s (R = 0.99 on average) and lowest between measurements made at 60 and 177 s (R = 0.92 on average). The strongest dependency was observed for parameter F_v'/F_m', while F_q'/F_v' showed the weakest dependency.

Fig. 5*C* maps the *Pearson*'s correlations between similar fluorescent parameters obtained at identical time points with different measurement techniques. As seen, correlations between the measurements at 690 and 735 nm made at the same time point are highly significant ($p<0.001$), and range between 0.70 and 0.91 with an average of 0.82. The correlations between parameters measured at either 690 or 735 nm and PAM measurements at the same time are far lower but still significant ($p<0.05$). One exception is F_q'/F_v', for which time series no observable correlations between the PAM and 690 nm responses were detected. The inter-dependencies of these rational parameters were weak to moderate ($0.48 < R < 0.65$), except for F_q'/F_m' to F_q'/F_v' in the F_{735} response and F_q'/F_m' to F_v'/F_m' in the F_{PAM} response ($R > 0.78$).

Crop measurements: As seen from Eq. 4 and Eq. 6, both LAI(t) and LUE can be determined from periodic destructive measurements and the corresponding greenhouse environmental data as crop model inputs. To avoid or at least minimize the number of required destructive harvests, a better approach is estimating them from other quantitative phenotypic traits. An imaging technique for LAI(t) estimation can be found in van der Heijden *et al.* (2012). To estimate LUE and yield related parameters for each genotype, genotypic means of the selected fluorescence traits were obtained then correlated to LUE and other phenotypic parameters (LAI, DM_{tot}, DM_{fruit}, DM_{leaf}, DM_{stem}, N_{fruit}, and η_{fruit}) obtained by destructive measurements.

Yield and total biomass production in the 40 genotypes varied highly. The average yield was DM_{fruit} = 80.1 g (± 27.5; 28.3; 140.5) of fruit per plant with standard deviation, minimum, and maximum values listed in brackets, respectively. Average total biomass per plant was DM_{tot} = 207.5 g (± 33.5; 140.8; 273.3). On average, there were N_{fruit} = 36.0 (± 11.9; 15; 60) fruits per plant and η_{fruit} = 38.1% (± 10.6; 14; 59) of the dry matter was partitioned into the fruits. Leaf area at the final destructive harvest was LAI = 8,616 cm^2 (± 2,150; 5,243; 14,255) and light-use efficiency was LUE = 1.24 g MJ^{-1} (± 0.15; 0.95; 1.56).

Yield is highly and significantly correlated to DM_{tot} (R = 0.61), η_{fruit} (R = 0.88), and N_{fruit} (R = 0.62), all at $p<0.001$. However, a larger number of fruits does not automatically result in a higher yield, as DM_{fruit} and N_{fruit} had an intermediate correlation (R = 0.48, p=0.003) due to the variation in fruit size (data not shown).

The crop measurements of the current SP3 experiment were compared to the ones reported by Alimi *et al.* (2013b) for SP2. The correlations of crop measurement parameters in the two experiments were high and significant ($p<0.001$ for all correlations), ranging from 0.71 for total biomass to 0.89 for number of fruits (Fig. 6*D*).

Heritability: Heritability values of all measurements were high, implying that large part of the variation was due to differences between the genotypes (Table 1). For the fluorescence measurements all rational parameters taken in the light-acclimated state except one ($F_q'1/F_v'1$ of the 690 nm response), more than 50% of the variation could be attributed to genotype, with 26 out of 27 parameters having a heritability of $H^2 > 0.5$. For absolute fluorescence values and F_v/F_m, seven out of the ten PAM responses showed low heritability values of $H^2 \leq 0.5$, whereas for DC responses, $H^2 > 0.5$ was observed for all values. Heritability values were higher for the crop measurements, in general above $H^2 = 0.8$.

Correlation between fluorescence and crop measurements: To identify fluorescence parameters that can be associated with crop measurements, correlation between fluorescence and crop parameters were calculated for a

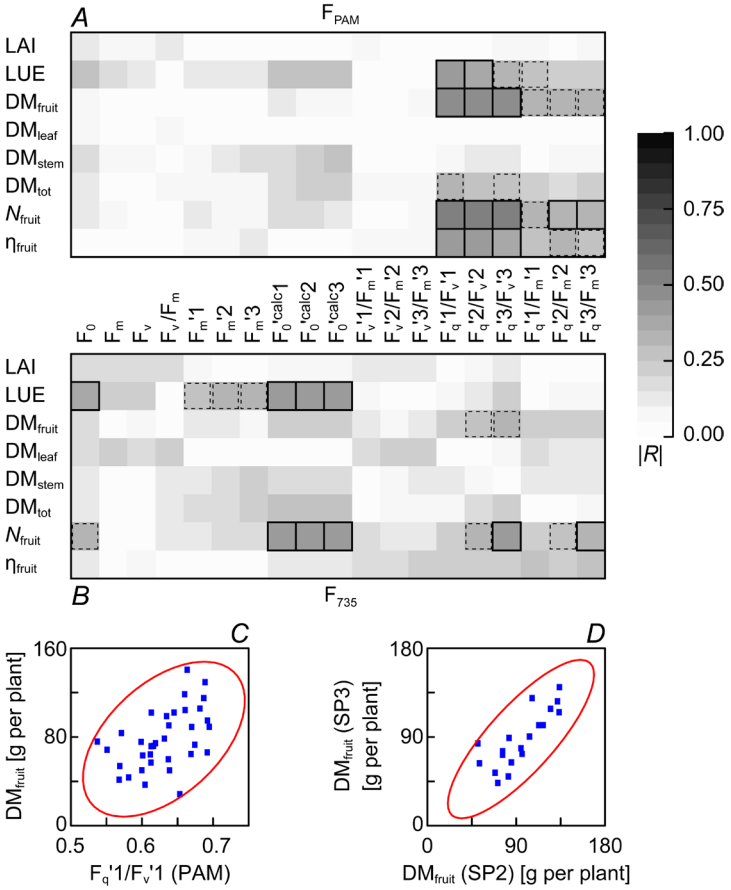

Fig. 6. (*A*,*B*) Correlation heat map of crop parameters to PAM and F_{735} DC fluorescence responses, respectively. Significant correlation levels at $p \leq 0.05$ are solid framed ($0.33 \leq |R| \leq 0.53$ for F_{PAM} and $0.37 \leq |R| \leq 0.42$ for F_{735}). Weaker values at significance of $0.05 < p < 0.1$ are dash framed ($0.28 \leq |R| \leq 0.32$ for both F_{PAM} and F_{735}). (*C*) Scatter plot of SP3 yield DM_{fruit} to $F_q'1/F_v'1$ of the PAM response with *Pearson*'s correlation coefficient of $R = 0.50$. (*D*) Scatter plot of SP2 to SP3 yields with maximum *Pearson*'s correlation coefficient of $R = 0.81$.

range of fluorescence parameters as plotted for PAM and F_{735} DC fluorescence responses in Fig. 6*A*,*B*, respectively. In general, these two maps revealed a complementary correlation structure so that correlations between absolute fluorescence parameters and crop data were not significant for PAM response, whereas correlations between rational fluorescence parameters and crop data were not high and often not significant for the DC responses. To the contrary, systematic correlations of a set of fluorescence parameters could be identified at high significance to LUE and fruit related parameters for all responses.

In case of DC responses, absolute fluorescence parameters yielded similar structures for F_{690} and F_{735} parameters with the latter (shown in Fig. 6*B*) having higher correlation values at higher significance. Significant correlations F_0 to LUE ($|R| = 0.29$ at $p=0.083$ for F_{690} and $|R| = 0.37$ at $p=0.024$ for F_{735}), $F_0'^{calc}i$ to LUE (average $|R| = 0.35$ at $p<0.05$ for F_{690} and $|R| = 0.41$ at $p=0.01$ for F_{735}) and $F_0'^{calc}i$ to N_{fruit} (average $|R| = 0.33$ at $p<0.05$ for F_{690} and $|R| = 0.43$ at $p<0.01$ for F_{735}) were identified.

Among the rational fluorescence parameters, the $F_v'i/F_m'i$ group was linked to η_{fruit} (average $R = 0.3$ at $p<0.1$) at 690 nm, whereas groups $F_q'i/F_v'i$ and $F_q'i/F_m'i$ were linked to N_{fruit} (average $R = 0.3$ at $p<0.1$) at 735 nm for $i \in \{2, 3\}$. Of these, $F_q'3/F_v'3$ showed the strongest correlation of $R = 0.4$ at $p=0.013$. Finally, at 735 nm, $F_q'2/F_v'2$ and $F_q'3/F_v'3$ were linked to LUE with $R = 0.28$ ($p<0.1$) and $R = 0.31$ ($p<0.1$), respectively.

At all three time points, PAM measurements of groups $F_q'i/F_v'i$ and $F_q'i/F_m'i$ correlated with yield (DM_{fruit}), N_{fruit}, and η_{fruit} at $p<0.1$ with *Pearson*'s coefficients ranging from 0.27 to 0.53. The strongest links were revealed between $F_q'i/F_v'i$ and N_{fruit} ($R \in \{0.51, 0.52, 0.53\}$ for $i \in \{1, 2, 3\}$ at $p \leq 0.002$) and between $F_q'i/F_v'i$ and DM_{fruit} ($R \in \{0.50, 0.48, 0.46\}$ for $i \in \{1, 2, 3\}$ at $p \leq 0.005$). A scatter plot of yield with the strongest link is plotted in Fig. 6*C*. Beside links with the fruit related parameters, $F_q'i/F_v'i$ data of the PAM measurements also correlated significantly to LUE (with a maximum of $R = 0.42$ for $i = 1$ at $p=0.01$). The $F_v'i/F_m'i$ parameter group of the PAM measurements had no significant correlations to any of the crop parameters.

QTL analyses on fluorescence parameters: Multi-trait QTL analyses were conducted per group of absolute and rational parameters, ($F_m'i$, $F_v'i$, $F_0'^{calc}i$ and $F_q'i$) and ($F_v'i/F_m'i$, $F_q'i/F_v'i$ and $F_q'i/F_m'i$), respectively, at the three different time points in the light-acclimated phase with $i \in \{1, 2, 3\}$. The QTLs found are listed in Table 2 for each set of parameters. Parameters F_m', F_v', $F_0'^{calc}$ and $F_v'i/F_m'i$ have their dark-acclimated counterparts, hence these parameters have two sets of QTLs, with and without the dark measurements.

In general, absolute fluorescence parameters indicated several QTLs at 690 nm (with less or no QTL for the 735 nm and PAM responses), especially when combined

Table 1. Heritability values calculated for fluorescence and crop parameters. Time index $i \in \{1, 2, 3\}$ refers to time points at $t_i \in \{60, 117, 177$ s$\}$. *Boldfaced values* refer to fluorescence traits that show significant correlation to crop parameters at $p<0.1$. Those marked with (*) show QTL effect from the SP3 trial that colocate with QTLs found on the SP2 crop parameters. *Underlined cells* show those fluorescence traits that present significant correlation to those crop traits having colocated SP2 QTL with SP3 QTL of the same fluorescence trait. Parameters are defined in the Appendix.

Fluorescence parameter	i	Heritability H^2 F_{690}	F_{735}	F_{PAM}
F_0		**0.82**	**0.66**	0.48*
F_m		0.64	0.59	0.35
F_v		0.63	0.58	0.36
F_v/F_m		0.64*	0.64	0.50
F_m'	1	0.73	**0.71**	0.48
	2	0.77	**0.75**	0.46
	3	0.78	**0.76**	0.42
$F_0'^{calc}$	1	**0.82***	**0.79***	0.62*
	2	**0.82***	**0.79***	0.59*
	3	**0.82***	**0.79***	0.57*
F_v'/F_m'	1	**<u>0.74</u>***	0.66	0.59
	2	**<u>0.77</u>***	0.70	0.60
	3	**<u>0.78</u>***	0.72	0.59
F_q'/F_v'	1	0.46	0.63	**0.76***
	2	0.56	**0.69**	**0.79***
	3	0.60	**0.71**	**0.77***
F_q'/F_m'	1	**0.67**	0.82*	**0.67***
	2	0.71	**<u>0.85</u>***	**0.69***
	3	0.72	**<u>0.85</u>***	**0.67***

Crop parameter (H^2)					
DM_{tot}	DM_{fruit}	N_{fruit}	η_{fruit}	LUE	LAI
0.79	0.89	0.92	0.94	0.81	0.94

with the corresponding dark measurement. An exception is F_v' for which a single QTL was found at 735 nm that completely disappeared when combined with the dark measurement. Parameter group $F_0'^{calc}$ indicated two QTLs being consistent across the different responses, that is one QTL on linkage group P7 at position 53.8 cM was found at both DC responses, whereas that on linkage group P11 at position 65.0 cM (P11@65.0) was present at all three responses.

At 690 nm, F_q'/F_m' indicated two QTL on linkage group P1 at different positions. F_q'/F_v' indicated two very weak QTLs on linkage groups P1 and P8. F_v'/F_m' found one on linkage group P11 at position 65.0 cM explaining a rather strong part of the measured variation. When dark-acclimated F_v/F_m was also included, an additional QTL was detected on linkage group P6 (Fig. 7*A*). A combined analysis of all three parameter groups proved more powerful yielding additional QTLs at linkage groups and cM positions of P2@31.0, P2@79.9, P3@1.4, P4@15.8, P5@82.3 and P7@91.5, respectively (data not shown).

At 735 nm, F_q'/F_m' obtained five QTLs, of which one (P2@89.7) displayed a strong effect (Fig. 7*B*). F_q'/F_v' yielded two QTLs, at linkage groups P1 and P2. F_v'/F_m' gave one weak QTL effect on linkage group P2.

The PAM measurements of F_q'/F_m' and F_v'/F_m' gave no QTL. Group F_q'/F_v' gave one strong QTL effect at linkage group P11, position 66.9. When parameters were combined for analysis, $\{F_q'i/F_m'i, F_v'i/F_m'i\}$ gave one QTL at linkage group P11, position 76.8 (Fig. 7*C*) resulting from F_q'/F_m', while combination $\{F_q'i/F_m'i, F_q'i/F_v'i\}$ yielded many QTLs, at linkage groups and cM positions of P1@0.0, P6@79.0, P7@52.5, P10@60.1, P10@110.1 and P11@76.0 (Fig. 7*D*). The combined analysis of $\{F_v'i/F_m'i, F_q'i/F_v'i\}$ yielded two QTLs, at linkage groups and cM positions of P10@60.1 and P11@76.8 resulting from F_q'/F_v'.

Comparison with previously found QTLs determining crop parameters: QTLs determining the fluorescence parameters were compared to the QTLs found for crop traits by Alimi *et al.* (2013b) in the multi-trait and multi-environment analyses of SP2 experiment. In multi-environment analyses, SP2 was part of two locations (Spain and the Netherlands) and two seasons (autumn and spring). The QTL found in the analysis of fluorescence parameters on linkage group P6 at position 69.4 cM corresponds to trait-specific QTL effects found for N_{fruit}, η_{fruit} and LUE in multi-trait analysis at marker 216 (SP745). The QTL found on linkage group P7 at position 91.5 cM is close to the one found for yield (DM_{fruit}), η_{fruit} and LAI at linkage groups and cM positions of P7@93.8 at marker 249 (SP147). The QTL found in several analyses of fluorescence parameters on linkage group P11 at position 65.0 cM collocates to environment-specific QTL effect for η_{fruit} in multi-environment analysis at marker 382 (CDKE). Finally, the QTL found in combined analysis of PAM rational parameters on linkage group P11 at position 76.8 cM colocates to environment-specific QTL effect for DM_{leaf} in multi-environment analysis at marker 393 (SP170).

Discussion

The original application of plant fluorescence has been to investigate the photosynthetic system (Baker 2008, Murchie and Lawson 2013). Next to this more fundamental application, it is used to detect stresses in cultivations, caused by *e.g.*, nutrient deficiency (Thoren and Schmidhalter 2009), water deficiency (Kautz *et al.* 2014), toxins (Barócsi *et al.* 2003) or the occurrence of diseases (Chaerle *et al.* 2007, Mahlein *et al.* 2012). It is also used to screen populations, for example for sensitivity to heat stress (Cottee *et al.* 2012, Sharma *et al.* 2012) or drought tolerance (Georgieva *et al.* 2008, Boureima *et al.* 2012). Fluorescence measurements have also proven useful to analyse cold stress in winter for several sclerophyll Mediterranean plant species (Zunzunegui *et al.* 2005,

Table 2. List of all QTLs found for fluorescence trait sets by multi-trait analysis based on temporal grouping of fluorescence parameters. Time index $i \in \{1, 2, 3\}$ shows that all three time points were included in the analysis. For QTLs found on more complex grouping of different temporal sets, refer to the text. List in each {} refers to those fluorescence traits included in that particular analysis. QTLs are given as 'marker number (linkage group@position in cM)'. QTLs typed *boldface* are those explicitly found on crop parameters. Parameters are defined in the Appendix.

Trait	QTL(F_{690})	QTL(F_{735})	QTL(F_{PAM})
{$F_m'i$}	236 (07@52.5) 384 (11@66.9)	-	72 (02@83.1) 297 (08@73.8)
{F_m, $F_m'i$}	9 (01@39.5) 26 (01@109.7) 32 (01@166.6) 210 (06@49.9) 236 (07@52.5) 396 (11@77.5)	-	-
{$F_v'i$}	-	72 (02@83.1)	-
{F_v, $F_v'i$}	-	-	-
{$F_0^{'calc}i$}	237 (07@53.8) **382 (11@65.0)**	237 (07@53.8) **382 (11@65.0)**	**382 (11@65.0)**
{F_0, $F_0^{'calc}i$}	8 (01@30.1) 207 (06@15.1) 231 (07@34.6) 351 (10@29.3) 383 (11@66.4)	236 (07@52.5) 385 (11@67.2)	359 (10@69.0) **382 (11@65.0)**
{$F_q'i$}	236 (07@52.5) 384 (11@66.9)	-	-
{$F_v'i/F_m'i$}	382 (11@65.0)	72 (02@83.1)	-
{F_v/F_m, $F_v'i/F_m'i$}	210 (06@49.9) **382 (11@65.0)**	-	-
{$F_q'i/F_v'i$}	6 (01@16.6) 294 (08@70.0)	7 (01@17.8) 73 (02@83.1)	384 (11@66.9)
{$F_q'i/F_m'i$}	7 (01@17.8) 25 (01@104.0)	7 (01@17.8) 74 (02@89.7) 131 (03@129.7) 146 (03@180.4) **216 (06@69.4)**	-

2011). Several articles combine screening of populations with fluorescence measurements (Rousseau *et al.* 2013), some in combination with QTL analysis (Harbinson *et al.* 2012), to select the appropriate genotypes. This paper is an attempt to bring this last combination into practice with a full-grown greenhouse crop.

It is known that transient fluorescence responses – related to the OJIP parameters – carry information that can be linked to differences between plant species or variants (Tyystjärvi *et al.* 1999, Keränen *et al.* 2003). A number of such parameters have been obtained in a phenotyping experiment on 37 genotypes of a RIL pepper progeny from both the dark and light acclimated induction phases upon the application of an appropriate spectral and temporal excitation protocol. As expected, several of the fluorescence parameters displayed high genotypic heritability reaching a maximum of $H^2 = 0.85$ validating that the total variations of those parameters have a strong genotypic origin.

The highest heritability calculated for fluorescence parameters was found for F_q'/F_m' at 735 nm. This can be explained by the fact that this ratio shows the prompt fluorescence increase between two different excitation light levels relative to the highest. Thus, this is also a measure of functioning photosystems. Furthermore, in the case of the F_{735} response, these values are not additionally affected by the reabsorption which corrupts this relationship in case of the F_{690} response.

The PAM signals display the best heritability in case of parameter set F_q'/F_v', also called as photochemical quenching (q_P), giving a nonlinear indication of the proportion of open PSII reaction centres (Murchie and Lawson 2013). Lower, but still high heritability values can be obtained for the parameter set F_q'/F_m', which is the quantum yield of PSII electron transport in the light-acclimated phase (Φ_{PSII}) that estimates the efficiency at which light absorbed by PSII antenna system is used for photochemistry (Baker and Rosenquist 2004, Murchie and Lawson 2013). So, the proportion of the opened PSII reaction centres has a stronger genetic background than the quantum efficiency of photochemistry.

Compared to crop values in Table 1, the heritability, also interpreted as repeatability, of fluorescence parameters varied between 0.35 and 0.85, which was lower than

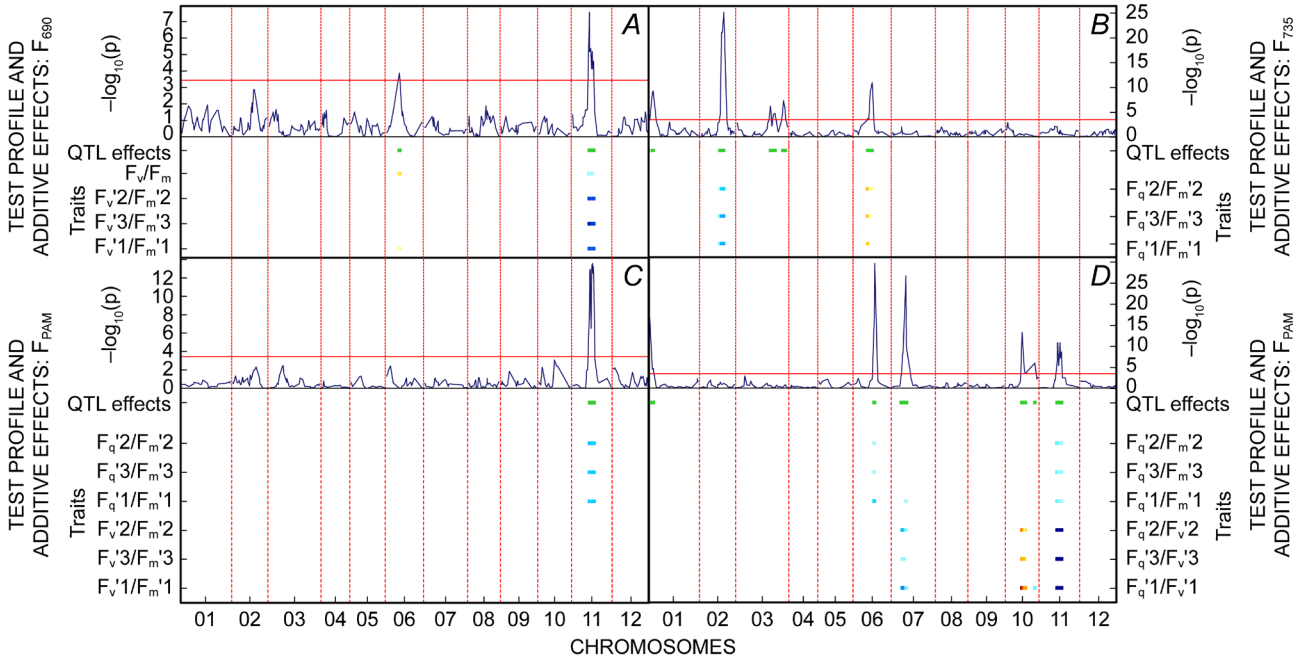

Fig. 7. (*A*) QTL profile for light acclimated 690 nm parameter group $F_v'i/F_m'i$ measured at $t_i \in \{60, 117, 177\ s\}$ with $i \in \{1, 2, 3\}$ including dark acclimated parameter F_v/F_m. (*B*) QTL profile for light acclimated 735 nm parameter group $F_q'i/F_m'i$. (*C*,*D*) QTL profiles for parameter combinations $\{F_q'i/F_m'i, F_v'i/F_m'i\}$ and $\{F_q'i/F_m'i, F_q'i/F_v'i\}$ of PAM fluorescence traits, respectively.

that for crop parameters varying between 0.79 and 0.94, possibly due to different scaling effects. One is due to the different time scales at which the variables are collected: the crop parameters are the results of four months of cultivation, while fluorescence responses are momentary measurements taken within two weeks, although the applied measurement scheme removed part of the effect. Another scale effect was measuring the whole plant compared to a single leaf. Such ranges and differences are consistent to those reported previously: repeatability of Φ_{PSII} found by Strigens *et al.* (2013) in maize varied between 0.39 and 0.60 among groups of inbred lines under optimal temperatures, whereas F_v/F_m had higher values ranging from 0.58 to 0.82. In their case, repeatability of crop measurements was also higher ranging from 0.80 to 0.97. Nevertheless, the progeny used in the experiments was the outcome of a cross between a domesticated and an exotic pepper. That made that all anatomical, morphological and physiological traits showed high H^2 because in the offspring there were always strongly contrasting genotypes. It is expected that this contrast is less for fluorescence parameters, where the parents are not expected to be as extreme as for the more standard traits.

Despite of the differences between fluorescence and crop measurements in the scale of time and space, significant positive correlations were observed between fluorescence trait group $F_q'i/F_v'i$ ($i \in \{1, 2, 3\}$) of the PAM response and all fruit related crop traits as well as LUE at moderate *Pearson*'s correlation R levels of 0.53, 0.50, 0.42, and 0.41 taking N_{fruit} to $F_q'3/F_v'3$, DM_{fruit} to $F_q'1/F_v'1$, η_{fruit} to $F_q'1/F_v'1$, and LUE to $F_q'1/F_v'1$, respectively, those with the highest correlation values from each temporal set (Fig. 6). In addition to the PAM response, the total fluorescence is also measured and an extra trait group $F_0'^{calc}i$ of the 735 nm DC response is also identified having significant negative correlation to N_{fruit} (R = –0.43) and LUE (R = –0.42). Similar trend with lower correlation values was identified for the 690 nm DC response. These fluorescence traits can be selected as proxies to crop model parameters noting that they themselves are complex traits (Stirbet *et al.* 2018). Another option is to add them as extra inputs for a crop model to derive (or validate) yield from different component traits.

Multi-trait QTL analysis of a number of fluorescence traits revealed several QTLs on all three fluorescence responses as listed in Table 2 for the simple temporally grouped traits. In general, QTLs were identified in those temporal trait sets showing the highest heritability as marked in Table 1. To reveal more or stronger QTLs, especially for the PAM response, more complex grouping of fluorescence traits was necessary due to the rather small number of genotypes (37) used in the QTL analyses compared to that usually used (*e.g.*, in Barchi *et al.* 2007, Bonnet *et al.* 2007, Alimi *et al.* 2013b, Murchie and Lawson 2013). For the DC fluorescence responses, more QTLs were found taking the simple multi-trait grouping of the same parameter measured at different times despite of the fact affecting the power of a QTL analysis that there were high pairwise correlations between the different temporal values (Fig. 5*A*,*B*).

QTLs of the fluorescence parameters of the present SP3 trial were comparable to the QTLs found for crop traits obtained by Alimi *et al.* (2013b) in the multi-trait and multi-environment analyses of SP2 trial despite of the

fact that only a common set of 19 genotypes were present in both trials. QTL effects found for N_{fruit}, η_{fruit} and LUE at marker 216 (SP745) can be linked to QTL of fluorescence trait set F_q'/F_m' that also gives significant correlation to N_{fruit}. The QTL found close to the one for yield (DM_{fruit}), η_{fruit} and LAI at marker 249 (SP147) can be colocated with QTL of the combined fluorescence trait set {F_v'/F_m', F_q'/F_v', F_q'/F_m'} of the 690 nm DC fluorescence response that also gives significant correlation between F_v'/F_m' and η_{fruit}. Finally, the QTLs found for several fluorescence parameters (especially for $F_0'^{calc}$ in all responses and F_v'/F_m' in the 690 nm response) at marker 382 (CDKE) also colocates to environment-specific QTL effect for η_{fruit} in multi-environment analysis.

The fact that common QTLs are found for fluorescence and crop traits indicates that these QTLs affect both processes on both long and short term.

Based on the trend of the heritability and correlation values (Table 2 and Fig. 5, respectively), it can be concluded that short-term fluorescence parameters recorded within 1 min after the onset of the actinic light of the fluorescence response curve can be selected as suitable traits for estimating the associated component trait. Moreover, the finding, that parameters $F_0'1$ (before actinic light) and $F_0'2$ (after actinic light) of the PAM response are identical ($R^2 > 0.92$; Fig. 3*C*) gives a proof of successfully forcing the sample to a uniform condition using the FR pulse even if the dark acclimation phase is shortened. Combining these two conditions offers a protocol for fast phenotyping on a timescale reduced to less than a minute, yet providing a complete set of fluorescence traits with physiological relevance.

The available set of traits can be extended if those of the total fluorescence responses are included in the analyses. As found, the most important is the parameter $F_0'^{calc}$ that can be calculated for both the PAM and DC responses. Taking the PAM response, its acceptable correlation to the measured $F_0'1$ values (Fig. 3*D*) is a proof of its physiological relevance as well as of the stable environmental conditions of the present large scale greenhouse experiment.

In conclusion, application of the IFS, a fast, nondestructive instrument for fluorescence measurements has been introduced as a phenotyping tool. The IFS has proven to obtain consistent data with high heritabilities. Although correlations between fluorescence parameters and crop measurements were moderate in the same experiment, QTLs of fluorescence parameters at linkage groups P6, P7, and P11 were either the same as for the yield components number of fruits, partitioning into the fruits, and light-use efficiency or close to that found for the complex trait yield in a similar experiment. This demonstrates that a fluorosensor can be a valuable addition to the existing crop breeding tools. Application of the fluorescence parameters in crop phenotyping and breeding may cover the testing plants' response to environmental conditions (such as temperature, radiation, water coverage and herbicides or other phytotoxic materials; Kalaji *et al.* 2018), optimizing growth environment of such environmental factors by regression models (Kim *et al.* 2006), revealing genetic variations and QTLs for photosynthetic traits (Poormohammad Kiani *et al.* 2008, Prinzenberg *et al.* 2018) to identify targets for breeding, chlorophyll fluorescence imaging to phenotype photosynthesis dynamics (McAusland *et al.* 2019), or determining their relationship to yield components (Czyczyło-Mysza *et al.* 2013, Noga *et al.* 2017). Most of these applications use the OJIP parameters, or a subset of the presented fluorescence traits. Utilizing several fluorescence traits simultaneously offers the advantage of forming more robust proxies as 'cheap' model inputs to replace one or more costly yield components.

References

Alimi N.A., Bink M.C.A.M., Dieleman J.A. *et al.*: Genetic and QTL analyses of yield and a set of physiological traits in pepper. – Euphytica **190**: 181-201, 2013a.

Alimi N.A. Bink M.C.A.M., Dieleman J.A. *et al.*: Multi-trait and multi-environment QTL analyses of yield and a set of physiological traits in pepper. – Theor. Appl. Genet. **126**: 2597-2625, 2013b.

Bąba W., Kompała-Bąba A., Zabochnicka-Świątek M. *et al.*: Discovering trends in photosynthesis using modern analytical tools: More than 100 reasons to use chlorophyll fluorescence. – Photosynthetica **57**: 668-679, 2019.

Baker N.R.: Chlorophyll fluorescence: a probe of photosynthesis *in vivo*. – Annu. Rev. Plant Biol. **59**: 89-113, 2008.

Baker N.R., Rosenquist E.: Applications of chlorophyll fluorescence can improve crop production strategies: an examination of future possibilities. – J. Exp. Bot. **55**: 1607-1621, 2004.

Barbagallo R.P., Oxborough K., Pallett K.E., Baker N.R.: Rapid noninvasive screening for perturbations of metabolism and plant growth using chlorophyll fluorescence imaging. – Plant Physiol. **132**: 485-493, 2003.

Barchi L., Bonnet J., Boudet C. *et al.*: A high-resolution, intraspecific linkage map of pepper (*Capsicum annuum* L.) and selection of reduced recombinant inbred line subsets for fast mapping. – Genome **50**: 51-60, 2007.

Barócsi A.: Intelligent, net or wireless enabled fluorosensors for mass monitoring of assorted crops. – Meas. Sci. Technol. **24**: 025701, 2013.

Barócsi A., Csintalan Z., Kocsányi L. *et al.*: Optimizing phytoremediation of heavy metal-contaminated soil by exploiting plants' stress adaptation. – Int. J. Phytoremediat. **5**: 13-23, 2003.

Barócsi A., Kocsányi L., Várkonyi S. *et al.*: Two-wavelength, multipurpose, truly portable chlorophyll fluorometer and its application in field monitoring of phytoremediation. – Meas. Sci. Technol. **11**: 717-729, 2000.

Bertin N., Martre P., Génard M. *et al.*: Under what circumstances can process-based simulation models link genotype to phenotype for complex traits? Case study of fruit and grain quality traits. – J. Exp. Bot. **614**: 955-967, 2010.

Boer M.P., Wright D., Feng L. *et al.*: A mixed-model quantitative trait loci (QTL) analysis for multiple-environment trial data using environmental covariables for QTL-by-environment interactions, with an example in maize. – Genetics **177**: 1801-1813, 2007.

Bonnet J., Danan S., Boudet C. *et al.*: Are the polygenic architectures of resistance to *Phytophthora capsici* and *P. parasitica* independent in pepper? – Theor. Appl. Genet. **115**: 253-264, 2007.

Boote K.J., Kropff M.J., Bindraban P.S.: Physiology and modelling of traits in crop plants: implications for genetic improvement. – Agr. Syst. **70**: 395-420, 2001.

Boureima S., Oukarroum A., Diouf M. *et al.*: Screening for drought tolerance in mutant germplasm of sesame (*Sesamum indicum*) probing by chlorophyll *a* fluorescence. – Environ. Exp. Bot. **81**: 37-43, 2012.

Bürling K., Cerovic Z.G., Cornic G. *et al.*: Fluorescence-based sensing of drought-induced stress in the vegetative phase of four contrasting wheat genotypes. – Environ. Exp. Bot. **89**: 51-59, 2013.

Buschmann C.: Variability and application of the chlorophyll fluorescence emission ratio red/far-red of leaves. – Photosynth. Res. **92**: 261-271, 2007.

Bustos-Korts D., Malosetti M., Chapman S., van Eeuwijk F.: Modelling of genotype by environment interaction and prediction of complex traits across multiple environments as a synthesis of crop growth modelling, genetics and statistics. – In: Yin X., Struik P.C. (ed.): Crop Systems Biology. Pp. 55-82. Springer, Cham 2016.

Cerovic Z.G., Masdoumier G., Ghozlen N.B., Latouche G.: A new optical leaf-clip meter for simultaneous non-destructive assessment of leaf chlorophyll and epidermal flavonoids. – Physiol. Plantarum **146**: 251-260, 2012.

Chaerle L., Lenk S., Hagenbeek D. *et al.*: Multicolor fluorescence imaging for early detection of the hypersensitive reaction to tobacco mosaic virus. – Plant Physiol. **164**: 253-262, 2007.

Chenu K., Chapman S.C., Tardieu F. *et al.*: Simulating the yield impacts of organ-level quantitative trait loci associated with drought response in maize: a "gene-to-phenotype" modeling approach. – Genetics **183**: 1507-1523, 2009.

Cottee N.S., Bange M.P., Wilson I.W., Tan D.K.Y.: Developing controlled environment screening for high-temperature tolerance in cotton that accurately reflects performance in the field. – Funct. Plant Biol. **39**: 670-678, 2012.

Czyczyło-Mysza I., Tyrka M., Marcińska I. *et al.*: Quantitative trait loci for leaf chlorophyll fluorescence parameters, chlorophyll and carotenoid contents in relation to biomass and yield in bread wheat and their chromosome deletion bin assignments. – Mol. Breeding **32**: 189-210, 2013.

Flood P.J., Kruijer W., Schnabel S.K. *et al.*: Phenomics for photosynthesis, growth and reflectance in *Arabidopsis thaliana* reveals circadian and long-term fluctuations in heritability. – Plant Methods **12**: 14, 2016.

Furbank R.T.: Plant phenomics: from gene to form and function. – Funct. Plant Biol. **36**: V-VI, 2009.

Furbank R.T., Tester M.: Phenomics – technologies to relieve the phenotyping bottleneck. – Trends Plant Sci. **16**: 635-644, 2011.

Georgieva K., Lenk S., Buschmann C.: Responses of the resurrection plant *Haberlea rhodopensis* to high irradiance. – Photosynthetica **46**: 208-215, 2008.

Harbinson J., Prinzenberg A.E., Kruijer W., Aarts M.G.M.: High throughput screening with chlorophyll fluorescence imaging and its use in crop improvement. – Curr. Opin. Biotech. **23**: 221-226, 2012.

Huot Y., Babin M.: Overview of fluorescence protocols: theory, basic concepts and practice. – In: Suggett D., Prášil O., Borowitzka M. (ed.): Chlorophyll *a* Fluorescence in Aquatic Sciences: Methods and Applications. Developments in Applied Phycology. Pp. 31-74. Springer, Dordrecht 2010.

Kalaji H.M., Rastogi A., Živčák M. *et al.*: Prompt chlorophyll fluorescence as a tool for crop phenotyping: an example of barley landraces exposed to various abiotic stress factors. – Photosynthetica **56**: 953-961, 2018.

Kautz B., Noga G., Hunsche M.: Sensing drought- and salinity-imposed stresses on tomato leaves by means of fluorescence techniques. – Plant Growth Regul. **73**: 279-288, 2014.

Keränen M., Aro E.-M., Tyystjärvi E., Nevalainen O.: Automatic plant identification with chlorophyll fluorescence fingerprinting. – Precis. Agric. **4**: 53-67, 2003.

Kim K.-S., Giacomelii G.A., Sase S. *et al.*: Optimization of growth environment in a plant production facility using a chlorophyll fluorescence method. – JARQ-Jpn. Agr. Res. Q. **40**: 149-156, 2006.

Kolukisaoglu Ü., Thurow K.: Future and frontiers of automated screening in plant sciences. – Plant Sci. **178**: 476-484, 2010.

Kuijken R.C.P, van Eeuwijk F.A., Marcelis L.F.M., Bouwmeester H.J.: Root phenotyping: from component trait in the lab to breeding. – J. Exp. Bot. **66**: 5389-5401, 2015.

Mahlein A.-K., Steiner U., Hillnhütter C. *et al.*: Hyperspectral imaging for small-scale analysis of symptoms caused by different sugar beet diseases. – Plant Methods **8**: 3, 2012.

Marcelis L.F.M., Elings A., Bakker M.J. *et al.*: Modelling dry matter production and partitioning in sweet pepper. – Acta Hortic. **718**: 121-128, 2006.

Marcelis L.F.M., Heuvelink E., Goudriaan J.: Modelling biomass production and yield of horticultural crops: a review – Sci. Hortic.-Amsterdam **74**: 83-111, 1998.

Marcial L., Sarrafi A.: Genetic analysis of some chlorophyll fluorescence and productivity parameters in barley *Hordeum vulgare*. – Plant Breeding **115**: 339-342, 1996.

Maxwell K., Johnson G.N.: Chlorophyll fluorescence – a practical guide. – J. Exp. Bot. **51**: 659-668, 2000.

McAusland L., Atkinson J.A., Lawson T., Murchie E.H.: High throughput procedure utilising chlorophyll fluorescence imaging to phenotype dynamic photosynthesis and photoprotection in leaves under controlled gaseous conditions. – Plant Methods **15**: 109, 2019.

Miloslavina Y., Wehner A., Lambrev P.H. *et al.*: Far-red fluorescence: A direct spectroscopic marker for LHCII oligomer formation in non-photochemical quenching. – FEBS Lett. **582**: 3625-3631, 2008.

Mishra A., Matouš K., Mishra K.B., Nedbal L.: Towards discrimi-nation of plant species by machine vision: Advanced statistical analysis of chlorophyll fluorescence transients. – J. Fluoresc. **19**: 905-913, 2009.

Montes J.M., Melchinger A.E., Reif J.C.: Novel throughput phenotyping platforms in plant genetic studies. – Trends Plant Sci. **12**: 433-436, 2007.

Murchie E.H., Lawson T.: Chlorophyll fluorescence analysis: a guide to good practice and understanding some new applications. – J. Exp. Bot. **64**: 3983-3998, 2013.

Noga A., Warchoł M., Czyczyło-Mysza I. *et al.*: Chlorophyll a fluorescence parameters in the evaluation of oat DH lines yield components. – Cereal Res. Commun. **45**: 665-674, 2017.

Oakey H., Verbyla A., Pitchford W. *et al.*: Joint modeling of additive and non-additive genetic line effects in single field trials. – Theor. Appl. Genet. **113**: 809-819, 2006.

Oxborough K., Baker N.R.: Resolving chlorophyll *a* fluorescence images of photosynthetic efficiency into photochemical and non-photochemical components – calculation of qP and F_v'/F_m' without measuring F_o'. – Photosynth. Res. **54**: 135-142, 1997.

Palombi L., Cecchi G., Lognoli D. *et al.*: A retrieval algorithm to evaluate the Photosystem I and Photosystem II spectral contributions to leaf chlorophyll fluorescence at physiological temperatures. – Photosynth. Res. **108**: 225-239, 2011.

Pedrós R., Goulas Y., Jacquemond S. *et al.*: FluorMODleaf: A new leaf fluorescence emission model based on the PROSPECT model. – Remote Sens. Environ. **114**: 155-167, 2010.

Pfündel E.: Estimating the contribution of Photosystem I to total leaf chlorophyll fluorescence. – Photosynth. Res. **56**: 185-195, 1998.

Poormohammad Kiani S., Maury P., Sarrafi A., Grieu P.: QTL analysis of chlorophyll fluorescence parameters in sunflower (*Helianthus annuus* L.) under well-watered and water-stressed conditions. – Plant Sci. **175**: 565-573, 2008.

Prinzenberg A.E., Víquez-Zamora M., Harbinson J. *et al.*: Chlorophyll fluorescence imaging reveals genetic variation and loci for a photosynthetic trait in diploid potato. – Physiol. Plantarum **164**: 163-175, 2018.

Richards R.A., Rebetzke G.J., Condon A.G., van Herwaarden A.F.: Breeding opportunities for increasing the efficiency of water use and crop yield in temperate cereals. – Crop Sci. **42**: 111-121, 2002.

Rousseau C., Belin E., Bove E. *et al.*: High throughput quantitative phenotyping of plant resistance using chlorophyll fluorescence image analysis. – Plant Methods **9**: 17, 2013.

Ruts T., Matsubara S., Walter A.: Synchronous high-resolution phenotyping of leaf and root growth in *Nicotiana tabacum* over 24-h periods with GROWMAP-plant. – Plant Methods **9**: 2, 2013.

Schreiber U., Klughammer C., Kolbowski J.: Assessment of wavelength-dependent parameters of photosynthetic electron transport with a new type of multi-color PAM chlorophyll fluorometer. – Photosynth. Res. **113**: 127-144, 2012.

Sharma D.K., Andersen S.B., Ottosen C.-O., Rosenqvist E.: Phenotyping of wheat cultivars for heat tolerance using chlorophyll *a* fluorescence. – Funct. Plant Biol. **39**: 936-947, 2012.

Shibu M.E., Leffelaar P.A., van Keulen H., Aggarwal P.K.: LINTUL3, a simulation model for nitrogen-limited situations: Application to rice. – Eur. J. Agron. **32**: 255-271, 2010.

Solti Á., Lenk S., Mihailova G. *et al.*: Effects of habitat light conditions on the excitation quenching pathways in desiccating *Haberlea rhodopensis* leaves: An Intelligent FluoroSensor study. – J. Photoch. Photobio. B **130**: 217-225, 2014.

Song Y., Glasbey C.A., Horgan G.W. *et al.*: Automatic fruit recognition and counting from multiple images. – Biosyst. Eng. **118**: 203-215, 2014.

Stirbet A., Lazár D., Kromdijk J., Govindjee: Chlorophyll *a* fluorescence induction: Can just a one-second measurement be used to quantify abiotic stress responses? – Photosynthetica **56**: 86-104, 2018.

Strasser R.J., Srivastava A., Govindjee: Polyphasic chlorophyll *a* fluorescence transient in plants and cyanobacteria. – Photochem. Photobiol. **61**: 32-42, 1995.

Strasser R.J., Srivastava A., Tsimilli-Michael M.: The fluorescence transient as a tool to characterize and screen photosynthetic samples. – In: Yunus M., Pathre U., Mohanty P. (ed.): Probing Photosynthesis: Mechanisms, Regulation and Adaptation. Pp. 445-483. Taylor & Francis, London 2000.

Strigens A., Freitag N.M., Gilbert X. *et al.*: Association mapping for chilling tolerance in elite flint and dent maize inbred lines evaluated in growth chamber and field experiments. – Plant Cell Environ. **36**: 1871-1887, 2013.

Thoren D., Schmidhalter U.: Nitrogen status and biomass determination of oilseed rape by laser-induced chlorophyll fluorescence. – Eur. J. Agron. **30**: 238-242, 2009.

Tyystjärvi E., Koski A., Keränen M., Nevalainen O.: The Kautsky curve is a built-in barcode. – Biophys. J. **77**: 1159-1167, 1999.

Tyystjärvi E., Nørremark M., Mattila H. *et al.*: Automatic identification of crop and weed species with chlorophyll fluorescence induction curves. – Precis. Agric.**12**: 546-563, 2011.

van der Heijden G., Song Y., Horgan G. *et al.*: SPICY: towards automated phenotyping of large pepper plants in the greenhouse. – Funct. Plant Biol. **39**: 870-877, 2012.

van Eeuwijk F.A, Bink M.C.A.M., Chenu K., Chapman S.C.: Detection and use of QTL for complex traits in multiple environments. – Curr. Opin. Plant Biol. **13**: 193-205, 2010.

van Eeuwijk F.A., Bustos-Korts D.V., Malosetti M.: What should students in plant breeding know about the statistical aspects of genotype × environment interactions? – Crop Sci. **56**: 2119-2140, 2016.

van Ittersum M.K., Leffelaar P.A., van Keulen H. *et al.*: On approaches and applications of the Wageningen crop models. – Eur. J. Agron. **18**: 201-234, 2003.

van Rooijen R., Kruijer W., Boesten R. *et al.*: Natural variation of *YELLOW SEEDLING1* affects photosynthetic acclimation of *Arabidopsis thaliana*. – Nat. Commun. **81**: 1421, 2017.

Voorrips R.E., Palloix A., Dieleman J.A. *et al.*: Crop growth models for the -omics era: the EU-SPICY project. – In: Prohens J., Rodríguez-Burruezo A. (ed.): Advances in Genetics and Breeding of Capsicum and Eggplant: Proceedings of the XIVth EUCARPIA Meeting on Genetics and Breeding of Capsicum and Eggplant. Pp. 315-321. Editorial Universidad Politécnica de Valencia, Valencia 2010.

Yin X., Struik P.C., Kropff M.J.: Role of crop physiology in predicting gene-to-phenotype relationships. – Trends Plant Sci. **9**: 426-432, 2004.

Yin X., Struik P.C., van Eeuwijk F.A. *et al.*: QTL analysis and QTL-based prediction of flowering phenology in recombinant inbred lines of barley. – J. Exp. Bot. **56**: 967-976, 2005.

Zunzunegui M., Díaz Barradas M.C., Ain-Lhout F. *et al.*: To live or to survive in Doñana dunes: Adaptive responses of woody species under a Mediterranean climate. – Plant Soil **273**: 77-89, 2005.

Zunzunegui M., Díaz Barradas M.C., Ain-Lhout F. *et al.*: Seasonal physiological plasticity and recovery capacity after summer stress in Mediterranean scrub communities. – Plant Ecol. **212**: 127-142, 2011.

Appendix

Relevant design parameters of SP2 and SP3. Each row/column location refers to a single bag. Raw arrangement for the two blocks is BB(BT)^{4}B-B(TB)^{4}BB with border (B) and tested (T) rows giving a tested of eight and total of 22 rows.

Experiment	Blocks	Genotypes per block	Plots per block	Rows (tested)	Columns (per plot)	Plants per bag	Plants per plot	Test plants per plot	Plants per m^2
SP2	2	152	192	22 (8)	54 (1)	5	5	3	3
SP3	2	40	40	22 (8)	54 (3–4)	5	15–20	3	3

Definition of recorded plant fluorescence parameters and their physiological interpretation in case of PAM detection mode (based on Baker and Rosenquist 2004).

Fluorescence parameter	Definition	Physiological interpretation of PAM signal
F_0, F_0'	Minimal fluorescence from dark and light-acclimated leaf, respectively	Level of fluorescence when primary quinone electron acceptors of PSII (Q_A) are maximally oxidized (PSII reaction centres are open)
F_m, F_m'	Maximal fluorescence from dark and light-acclimated leaf, respectively	Level of fluorescence when Q_A is maximally reduced (PSII reaction centres are closed)
$F_v = F_m - F_0$, $F_v' = F_m' - F_0'2$	Variable fluorescence from dark and light-acclimated leaf, respectively	Demonstrates the ability of PSII to perform primary photochemistry, *i.e.*, photoreduction of Q_A
$F_q' = F_m' - F'$	Difference of F_m' and fluorescence F' from actinic-light-acclimated leaf	Photochemical quenching of fluorescence due to open PSII reaction centres
F_v/F_m	Maximum quantum efficiency of PSII photochemistry	Maximum efficiency at which light absorbed by light-harvesting antennae of PSII is converted to chemical energy (Q_A reduction)
F_v'/F_m'	PSII maximum efficiency	Estimates the maximum efficiency of PSII photochemistry at a given light intensity, which is the PSII operating efficiency if all the PSII centres were open (Q_A oxidized)
F_q'/F_m'	PSII operating efficiency	Estimates the quantum efficiency at which light absorbed by PSII antennae is used for photochemistry (Q_A reduction)
F_q'/F_v'	PSII efficiency factor (photochemical quenching)	Relates the PSII maximum efficiency to the PSII operating efficiency